Infrared studies of low-temperature symmetry breaking in the perrhenate family of ET-based organic molecular conductors

S. M. Baker, J. Dong, G. Li, Z. Zhu, and J. L. Musfeldt
Department of Chemistry, State University of New York at Binghamton, Binghamton, New York 13902–6016

J. A. Schlueter, M. E. Kelly, R. G. Daugherty, and J. M. Williams
Materials Science Division, Argonne National Laboratory, 9700 South Cass Avenue, Argonne, Illinois 60439
(Received 26 August 1998; revised manuscript received 22 January 1999)

The polarized infrared and optical reflectance spectra of several members of the bis-(ethylenedithio)-tetrathiafulvalene (ET) complexed with perrhenate class [$(ET)_2(ReO_4)$, α-$(ET)_3(ReO_4)_2$, β-$(ET)_3(ReO_4)_2$] of organic molecular solids have been measured as a function of temperature. For the compounds studied, the spectra are highly anisotropic, with data in the good conductivity polarization dominated by totally symmetric electron-phonon activated A_g modes of ET. The low-temperature phase of each material is characterized by the opening of a semiconducting gap and vibronic symmetry breaking, as evidenced by vibrational fine structure in varying degrees. The nature and splitting of the 900-cm^{-1} perrhenate mode through the phase-transition temperatures implies that anion ordering drives the phase transition in the two 3:2 phases whereas the 82-K metal $\rightarrow$ insulator transition in $(ET)_2(ReO_4)$ is a weak structural modification in which anion reordering plays a minimal role. Correlation effects in this set of compounds are important, suggesting that a Hubbard gap picture may be appropriate for interpreting the low-lying electronic structure in these organic molecular solids. [S0163-1829(99)01326-0]

I. INTRODUCTION

Over the past decade, there has been sustained interest in the charge-transfer salts which bis-(ethylenedithio)-tetrathiafulvalene (ET) forms with various counterions. Notable successes include the observation of superconductivity above 10 K in several materials (e.g., κ-$(ET)_2Cu(NCS)_2$, κ-$(ET)_2Cu[N(CN)_2]$).[1–3] At the same time, engineering of new organic building block and counterion molecules has been instrumental in the development of novel organic molecular conductors and superconductors.[4–6] In the design of these compounds, chemical structure modifications have yielded large variances in the physical properties displayed by each material. For instance, subtle differences in packing, order, and proximity of counterions can lead to compounds exhibiting a variety of ground states and a cornucopia of properties, including superconductivity.

In this investigation, we examine three members of the ET/perrhenate class of materials: $(ET)_2(ReO_4)$, α-$(ET)_3(ReO_4)_2$, and β-$(ET)_3(ReO_4)_2$. Of these three, the 2:1 phase has been studied most extensively due to its superconducting properties below 2 K at 4 kbar of pressure.[7,8] Early on, Parkin *et al.* suggested that the 82-K structural phase transition is associated with counterion (perrhenate) *reordering*; structural studies showed that the anions were already ordered at room temperature.[8] Such a conclusion was attractive based on the similarity with tetramethyltetraselenafulvalene (TMTSF) systems, where ordering of tetrahedral counterions proved to be so important. Later, electron-spin resonance (ESR) experiments attributed the first-order metal $\rightarrow$ insulator phase transition at 82 K to anion ordering as well, based upon similarities with the $(TMTSF)_2BF_4$ system.[9] More recently, Ravy *et al.* suggested that the phase transition is far more complex than previously believed.[10] From temperature-dependent structural investigations, certain x-ray crystallographic peaks (associated with anion ordering at 300 K) were found to be unaffected at T_c, indicating a less significant role for the counterion. This result, combined with large differences between the ET system as compared to the TMTSF series, led Ravy to conclude that $(ET)_2(ReO_4)$ undergoes a displacive phase transition, with large distortions to the organic stack as the driving mechanism.[10] Infrared and optical experiments, ideal for confirmation of unit-cell doubling and assessing the role of the counterion, have not been performed on the 2:1 ET compound.

In contrast, α-$(ET)_3(ReO_4)_2$ has been investigated by optical techniques. Yakushi *et al.* examined the infrared response of the α-3:2 material, with the goal of observing gap formation.[11] This compound displays a broad electronic maximum near 2000 cm^{-1} and a sharp peak at 1250 cm^{-1} in the conductivity spectrum. The broad structure at $\approx$2000 cm^{-1} was attributed to an interband transition because no dispersion corresponding to the charge-transfer between neighboring cations in the near-infrared region was observed.[11] ESR studies on α-$(ET)_3(ReO_4)_2$ phase suggest that, like the 2:1 phase, this organic conductor undergoes an electronic Peierls transition at 88 K. The presence of two distinct ESR lines at low temperature indicates some sort of symmetry breaking for α-$(ET)_3(ReO_4)_2$, with activated behavior observed as well.[9] β-$(ET)_3(ReO_4)_2$ is the least known of these three chemically similar compounds, with only a preliminary report of semiconducting behavior and a possible phase transition near 100 K.[12]

The structure of these crystals (Fig. 1) has been studied extensively in the past, making this family of perrhenate-

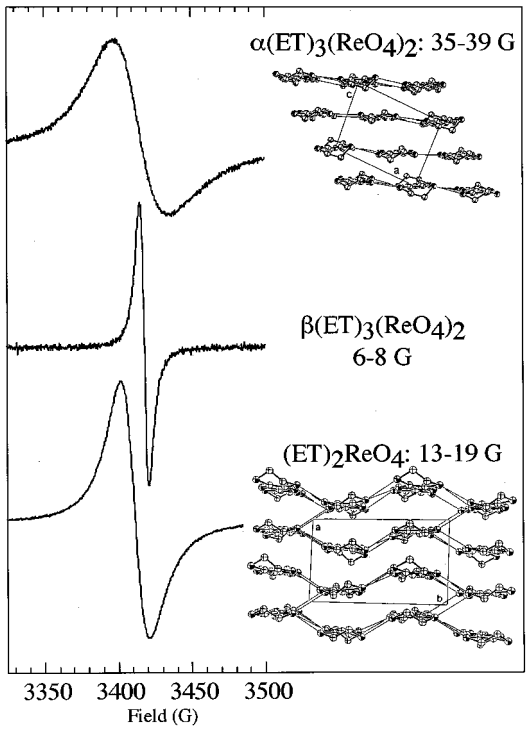

FIG. 1. Structure of the α, β, and 2:1 motifs for the ET/perrhenate family of organic molecular conductors, together with 300-K ESR linewidth data. Intermolecular contacts of less than 3.6 Å are shown.

based salts an excellent proving ground for chemical structure/physical property investigations.[2,7,8,13–18] Here, the simple tetrahedral nature of the counterion allows us to concentrate on the structural architecture of the solid as determined by the arrangement of the ET building block molecules. As with all ET complexes, the side to side *S*-*S* interactions are important. For the 2:1 salt, the ET molecules are arranged in a zigzagged motif perpendicular to the stacking direction, similar to the structure of $(TMTSF)_2X$ ($X = ClO_4^-$, AsF_6^-, PF_6^-, ReO_4^-).[7] For the α-3:2 phase, it is important to note that the α packing exhibited here is not the typical ''herringbone''-type α packing seen in most ET materials. Instead, all ET molecules lie parallel to each other, with six ET molecules per unit cell, arranged in two layers. As shown in Fig. 1, α-$(ET)_3(ReO_4)_2$ is a fairly two-dimensional material.[11] In contrast, the β structure has ET molecules arranged in a trimerized fashion along the stacking direction (note the 2/3 filling for both α and β phases). In several families of ET-based organic molecular conductors, β-type crystals often display superconductivity [e.g., β-$(ET)_2(I)_3$, β''-$(ET)_2SF_5CH_2CF_2SO_3$ (Refs. 4 and 19–21)]. However, there are large structural differences between these superconducting β-phase salts and the ET/perrhenate semiconducting β structure, mainly due to shorter interstack *S*-*S* contacts between the ET molecules in the superconductors. Also, studies on superconducting β-phase compounds report quasimetallic spectral behavior at room temperature, a moderate two-dimensionality, and a half filled band (based on the dimer) structure, all characteristics foreign to β-$(ET)_3(ReO_4)_2$.[22]

In order to explore the chemical structure/physical property relationships in the perrhenate-based family of ET molecular conductors, we have measured the infrared and optical reflectance spectra as a function of temperature and polarization. A Kramers-Kronig analysis was performed yielding optical constants from the reflectance data. Our overall goal is to obtain a microscopic understanding of the chemical structure/physical property relationships of these compounds, which may lead to development of techniques for the preparation of designed molecular materials and ultimately, to strategies for control of structure and properties in organic molecular solids.

II. EXPERIMENT

Single-crystal samples of $(ET)_2(ReO_4)$, α-$(ET)_3(ReO_4)_2$, and β-$(ET)_3(ReO_4)_2$ were electrocrystallized on Pt electrodes in a *H* cell containing 1,1,2-tetrabutylammonium perrhenate as the supporting electrolyte. As is typical for ET-based complexes, a variety of phases were obtained from the crystal-growth procedure.[12] Of the six known phases of the ET/perrhenate family, we were interested in three representative crystals, the 2:1 superconductor, and two of the three 3:2 isomers. The crystals of $(ET)_2(ReO_4)$, α-$(ET)_3(ReO_4)_2$, and β-$(ET)_3(ReO_4)_2$ had dimensions of $1.9\times1.6\times0.3$ mm^3, $2.8\times2.1\times0.2$ mm^3, and $2\times2\times0.3$ mm^3, respectively.[23] The various phases were easily identified using room-temperature ESR linewidth measurements as shown in Fig. 1.[9]

Near normal polarized reflectance measurements were made on the three samples with a Bruker 113 V (30 -5000 cm^{-1}), a Fourier transform spectrometer, and a Perkin-Elmer Lambda-900 ($4000-40000$ cm^{-1}), a grating instrument. For the far-infrared (FIR) measurements, a helium cooled bolometer detector was used to obtain an enhanced sensitivity. Traditional room-temperature detectors were employed over the middle- and near-infrared (MIR, NIR), optical, and ultraviolet (UV) range.

The measurements on each sample were taken in two polarizations, those of maximum anisotropy on the largest crystal face, allowing us to probe two of the three principle axes of the dielectric tensor. The optic axes were determined at 300 K. FIR and MIR measurements were made at a variety of temperatures, concentrating around the phase-transition temperature in each sample. For temperature control, we used an open flow cryostat mounted in the reflectance stage of the infrared spectrometer. Only room-temperature data were collected in the NIR/optical/UV range, providing a good extrapolation to the lower energy data for the Kramers-Kronig analysis.

A Kramers-Kronig analysis was performed to obtain the real and imaginary parts of the dielectric function, and thus the optical constants of each material [$\sigma_1(\omega)$, $\epsilon_1(\omega)$, $N_{eff}(m/m^*)$].[24] Note that ϵ_1 is the real (in-phase) part of the dielectric function and σ_1 is the imaginary, out-of-phase part. The high-frequency extrapolation to the Kramers-Kronig phase integral was done as ω^{-2}, and the low-frequency extrapolation to the phase-shift integral was made as a constant, or with a metallic Hagen-Rubens-type extrapolation, as appropriate for each salt. The available structural data were used to extract sum-rule information.[8,25]

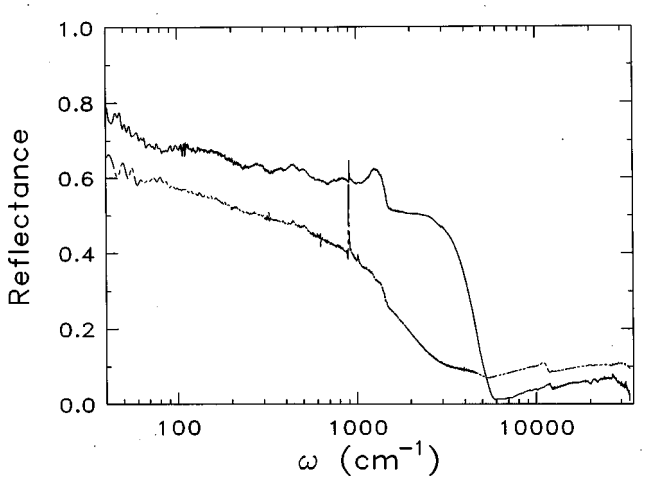

FIG. 2. Room-temperature reflectance of $(ET)_2(ReO_4)$. Solid line: ∥ polarization; dashed line: ⊥ polarization. Note the logarithmic frequency scale.

III. RESULTS

A. $(ET)_2(ReO_4)$

1. Room-temperature spectra

Figure 2 displays the 300-K reflectance of $(ET)_2(ReO_4)$ in the two principle polarization directions. Note that the overall reflectance is much less than unity at low frequencies and that considerable spectral anisotropy is present over the entire frequency range, both characteristics foreign to a Drude ''free-electron'' metal. In addition, screened vibronic features and low-lying electronic structure are observed along the stacking direction. Thus $(ET)_2(ReO_4)$ is best classified as a weak metal.

The vibrational response of organic molecular solids is fairly distinctive due to the electron-phonon coupling features which appear in the infrared spectra. The activation mechanism of the normally IR-inactive A_g vibrations involves electron-molecular vibrational coupling, in which a totally symmetric mode of the ET molecule couples to a low-lying electronic excitation or modulation of the charge density.[26–29] Such features display enhanced oscillator strength and can be highly polarized, often along the stacking direction of a crystal. For ET-based solids, normal mode calculations predict 12 A_g vibrations (assuming a planar D_{2h} point group) labeled ν_1 to ν_{12}.[30–32] In addition to the A_g modes, IR-allowed B_{1u}, B_{2u}, and B_{3u} vibrations[30–33] as well as electron-phonon coupling-allowed B_g modes[34,35] of the D_{2h} point group may appear.

Assignments of the A_g vibrations for all three perrhenate-based moieties appear in Table I. Note that for $(ET)_2(ReO_4)$, the high reflectance direction contains the aforementioned activated A_g modes, although they are well screened and some are not strong enough to be easily observed. Perpendicular to the stacking direction, $(ET)_2(ReO_4)$ displays a strong antisymmetric stretching mode of the anion at 900 cm^{-1},[36] but otherwise is bereft of significant features.

Figure 3 shows the room temperature frequency dependent conductivity of $(ET)_2(ReO_4)$, obtained via Kramers-Kronig analysis. Overall, the sample displays semimetallic character, with significant residual conductivity (but no free-carrier response) in the FIR, consistent with the moderate value of σ_{DC}.[12] The aforementioned A_g vibrational modes are observable but fairly well screened. At 300 K, a broad, low-energy electronic structure is centered near 1000 cm^{-1} in the stacking axis polarization. Additional correlation-induced bands and localized molecular excitations appear at higher energy.

TABLE I. A_g vibrational mode assignments from maxima in $\sigma_1(\omega)$ (in cm^{-1}) for $(ET)_2(ReO_4)$, α-$(ET)_3(ReO_4)_2$, and β-$(ET)_3(ReO_4)_2$. vs: very strong; s: strong; m: medium; w: weak; vw: very weak. Note that these are perturbed frequencies, taken from maxima in σ_1, as opposed to unperturbed frequencies.

Mode	$(ET)_2(ReO_4)$	α-$(ET)_3(ReO_4)_2$	β-$(ET)_3(ReO_4)_2$
ν_1	2980 (vw)	2940 (vw)	2963 (s)
ν_2	1554 (vw)	1550 (vw)	1552 (vw)
ν_3	1290 (m)	1296 (s)	1323 (vs)
ν_4	1415 (w)	1415 (w)	1404 (w)
ν_5	1280 (w)	1270 (m)	1278 (s)
ν_6	1006 (w)	1008 (w)	953 (w)
ν_7	902 (s)	900 (s)	902 (s)
ν_8	603 (vw)	649 (vw)	632 (vw)
ν_9	483 (m)	462 (m)	470 (m)
ν_{10}	448 (m)	447 (m)	448 (m)
ν_{11}	315 (w)	310 (vw)	306 (m)
ν_{12}	-	-	-

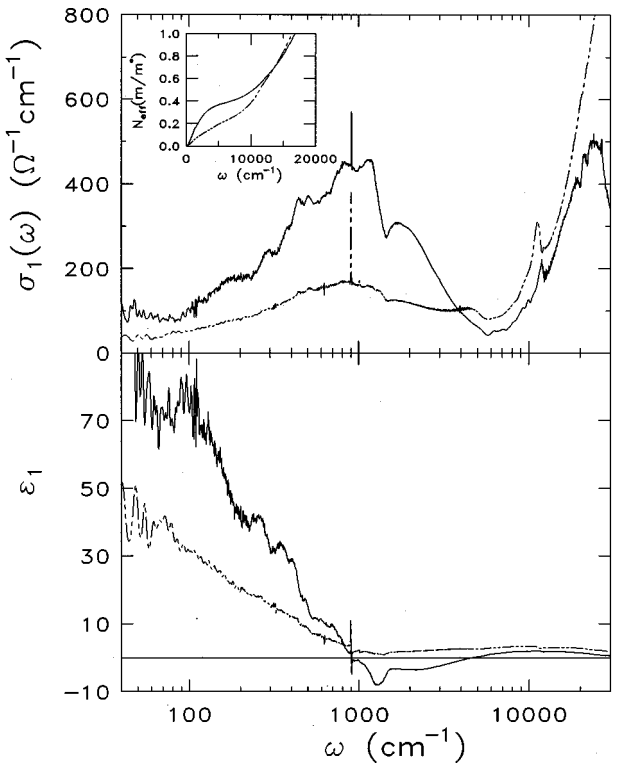

FIG. 3. Top panel: room-temperature frequency dependent conductivity of $(ET)_2(ReO_4)$. Solid line: ∥ polarization; dashed line: ⊥ polarization. Inset: 300-K conductivity sum rule in the ∥ and ⊥ polarizations, respectively. Bottom panel: room-temperature dielectric constant of $(ET)_2(ReO_4)$. Solid line: ∥ polarization; dashed line: ⊥ polarization.

Partial sum-rule data for the 2:1 phase appear as an inset in Fig. 3, providing information on the effective number of electrons involved in optical transitions [found from the area under the $\sigma(\omega)$ curve].[37] Here, we have calculated the sum rule on a ''per cluster basis,'' which facilitates comparison between the various perhennate samples studied here. It also allows us to avoid the problem of the detailed charge distribution in the cluster. Parallel to the stacking direction, $N_{eff}(m/m^*)$ rises sharply at low frequencies, levels off, and then increases more slowly throughout the region of measurement. We estimate $m^* \approx 2.9 m_e$ (where m_e is free-electron mass) from the leveling off of $N_{eff}(m/m^*)$ in the optical regime. An effective mass of this size in organic solids is generally taken as an indication of strong electron-electron correlations, although it can indicate minimal curvature of the Fermi surface at room temperature as well.

The lower panel of Fig. 3 shows the 300-K dielectric constant of $(ET)_2(ReO_4)$ in the two principle polarization directions. ϵ_1 is positive at low frequencies in the parallel polarization, consistent with the ''overdamped'' reflectance behavior. From the zero crossing of ϵ_1, we estimate $\omega_p \approx 4720\ cm^{-1}$. In the parallel direction, ϵ_1 is positive at low frequency, extrapolating to a static value of ≈ 70; in the $\perp$ direction, $\epsilon_1(0) \approx 40$. We are unaware of any low frequency dielectric results which might be used for comparison. $\epsilon_1(\infty)$ is ≈ 0.9 in the parallel direction and 1.2 in the perpendicular polarization, close to the expected value of $\epsilon_1(\infty) = 1$.

2. Temperature dependence

The 2:1 phase has a first-order metal $\rightarrow$ insulator transition at 82 K,[8,7] which is readily apparent in Fig. 4. Here, the stacking axis data for $(ET)_2(ReO_4)$ are at temperatures above and below the transition. The overall decrease in the FIR reflectance below T_c yields a semiconducting gap. Linear extrapolation of the leading edge of this band to the abscissa is well known to provide an estimate of the optical gap 2Δ. We estimate $2\Delta \approx 480\ cm^{-1}$ for $(ET)_2(ReO_4)$. This method of estimating the optical gap has error bars on the order of $\pm 100\ cm^{-1}$.

Only the FIR vibrational structures of $(ET)_2(ReO_4)$ display significant splitting in the low-temperature phase, reminiscent of $(TMTSF)_2(ReO_4)$.[36] While the ν_9 and ν_{10} regimes (near 450 cm^{-1}) exhibit strong splitting (see inset of Fig. 4), the area surrounding the central $C=C$ vibration displays only minor symmetry breaking. In the very FIR, lattice modes, similar to those in $(TMTSF)_2ReO_4$, are observed;[38] these will be discussed in detail in a later section. In the perpendicular direction, the anion mode at 900 cm^{-1} remains unsplit at 10 K. However, a quartet centered near 300 cm^{-1} becomes apparent in the parallel polarization at low temperature. This feature is attributed to a ReO_4 bending mode due to its similarity to a structure in $(TMTSF)_2(ReO_4)$.[36]

B. α-$(ET)_3(ReO_4)_2$

1. Room-temperature spectra

Figure 5 displays the near-normal polarized reflectance of α-$(ET)_3(ReO_4)_2$ at room temperature. Clearly, this is the response of an anisotropic two-dimensional conductor, with

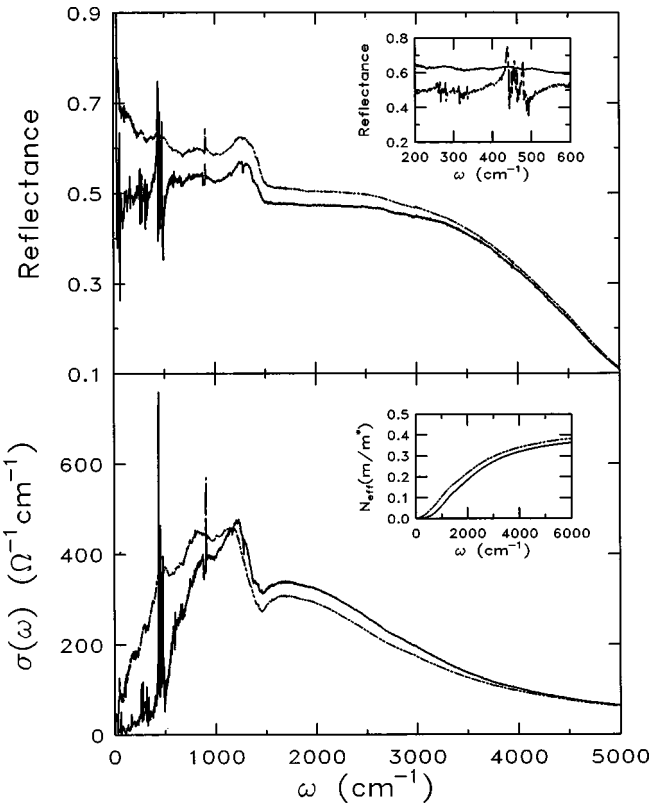

FIG. 4. Upper panel: reflectance of $(ET)_2(ReO_4)$ in the $\parallel$ polarization at 300 K (dashed line) and 10 K (solid line). Inset: ν_9 and ν_{10} splitting at 300 and 10 K. Lower panel: frequency dependent conductivity of $(ET)_2(ReO_4)$ in the $\parallel$ polarization at 300 K (dashed line) and 10 K (solid line). Inset: temperature dependence of the conductivity sum rule, 300 and 10 K.

reflectance higher along the [102] axis than perpendicular to it. Similar to the 2:1 phase, the overall shape of the high reflectivity direction indicates good conductivity at 300 K, although it is clearly not the response of a Drude ''free-electron'' metal. At the same time, vibrational features are reasonably well-screened, occurring predominantly parallel to the [102] plane shown in Fig. 5, but are moderately

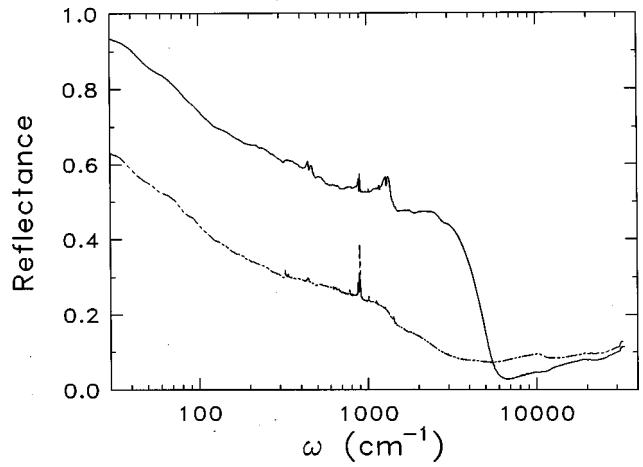

FIG. 5. Room-temperature reflectance spectra of α-$(ET)_3(ReO_4)_2$. Solid line: $\parallel$ polarization; dashed line: $\perp$ polarization. Note the logarithmic frequency scale.

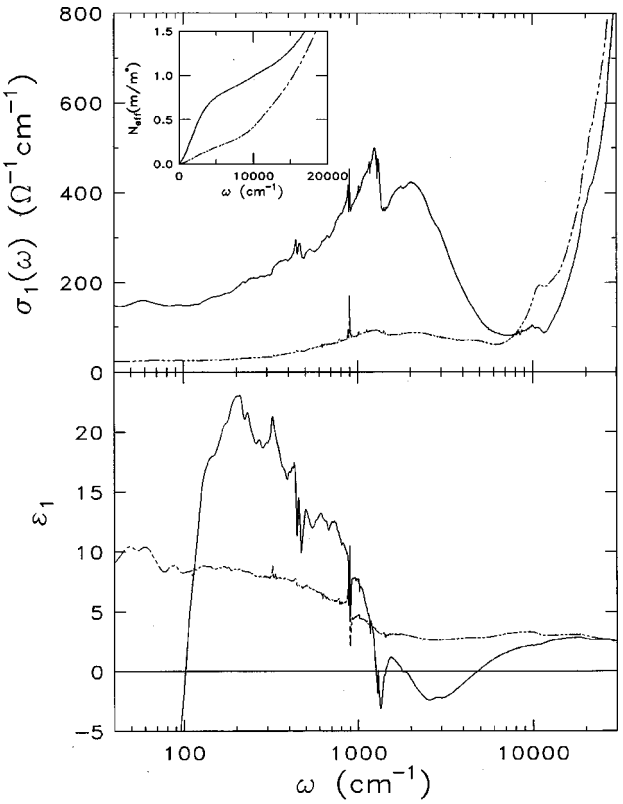

FIG. 6. Top panel: room-temperature conductivity of α-$(ET)_3(ReO_4)_2$. Solid line: $\|$ polarization; dashed line: $\perp$ polarization. Inset: 300 K conductivity sum rule as a function of polarization. Bottom panel: room-temperature dielectric constant of α-$(ET)_3(ReO_4)_2$. Solid line: $\|$ polarization; dashed line: $\perp$ polarization.

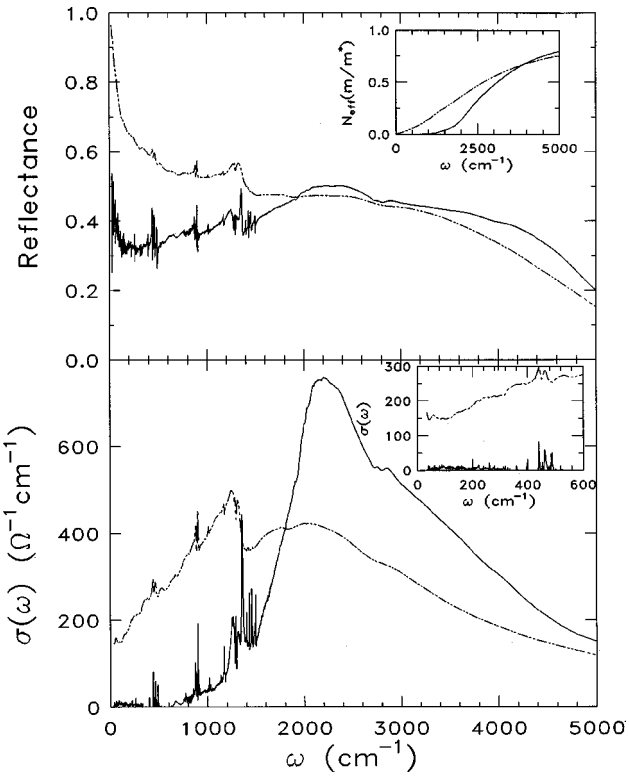

FIG. 7. Upper panel: reflectance of α-$(ET)_3(ReO_4)_2$ in the $\|$ polarization at 300 K (dashed line) and 10 K (solid line). Inset: temperature dependence of the sum rule, 300 and 10 K. Lower panel: frequency dependent conductivity of α-$(ET)_3(ReO_4)_2$ in the $\|$ polarization at 300 K (dashed line) and 10 K (solid line). Inset: FIR conductivity at 300 and 10 K.

present in the perpendicular direction as well.[11] A low-lying electronic structure is also observed in the middle infrared. Note that additional electronic excitations are observed at higher energy, with that centered near 10 000 cm^{-1} likely a correlation-induced band, and localized molecular excitations near 20 000 cm^{-1}.

Many of the structures observed in the infrared reflectance spectrum of α-$(ET)_3(ReO_4)_2$ can be attributed to A_g vibrational modes, activated by the well-known electron-phonon coupling process.[26–29] A unique trait of the α crystal is that some of the A_g vibrations appear in both polarizations, due to the fact that the ET molecules are arranged in a two-dimensional plane as opposed to a linear chain. As in $(ET)_2(ReO_4)$, the unusually strong feature at 900 cm^{-1} in the transverse direction is assigned to an anion mode.

Figure 6 displays the frequency dependent conductivity for α-$(ET)_3(ReO_4)_2$ in the two principle polarization directions. The overall shapes of the spectra suggest a weakly conducting response. In accord with previous spectroscopic work on this phase, an interesting electronic structure centered near 2200 cm^{-1} appears in the polarization parallel to [102].[11] Vibrational features are superimposed on this feature, with significant residual conductivity at low energy. From the partial sum-rule plot (inset Fig. 6), we find $m^* \approx 2.2 m_e$ in the high-conductivity direction.

The lower panel of Fig. 6 displays the 300-K frequency dependent dielectric constant of α-$(ET)_3(ReO_4)_2$. Parallel to [102] ϵ_1 dips sharply as it heads into the very FIR at 170 cm^{-1}, eventually turning negative near 110 cm^{-1}. The central $C=C$ vibration at 1270 cm^{-1} is the only phonon dispersion strong enough to drive the dielectric function to negative values. We extract a screened plasma frequency ω_p of 4250 cm^{-1}, compared with 9517 cm^{-1} obtained by Kuroda and co-workers.[11,39] This difference seems to arise from the method used to calculate ω_p; ours is determined from the zero crossing of ϵ_1.[24] In the perpendicular polarization, ϵ_1 rises slightly in the FIR, but is positive, fairly constant, and low over the entire frequency range. As expected for a low-dielectric semiconductor, extrapolation to zero frequency yields $\epsilon_1(0) \approx 10$ in the perpendicular polarization. Both polarizations give a high-frequency dielectric constant of 2.5.

2. Temperature dependence

Figure 7 displays the reflectance and frequency dependent conductivity of α-$(ET)_3(ReO_4)_2$ at temperatures above and below the metal $\rightarrow$ insulator transition in the polarization parallel to [102]. α-$(ET)_3(ReO_4)_2$ has a weakly metallic high-temperature phase and a low-temperature phase which displays a strong semiconducting gap structure. The semiconducting gap is clear in both polarizations, although somewhat sharper in the perpendicular direction. The beginning of this gap was also reported by Yakushi *et al.* in a previous spectroscopic study of α-$(ET)_3(ReO_4)_2$.[11] However, the previous measurements were not extended into the FIR region, so full development of the gap structure was not observed. From an extrapolation of the leading edge of this structure,

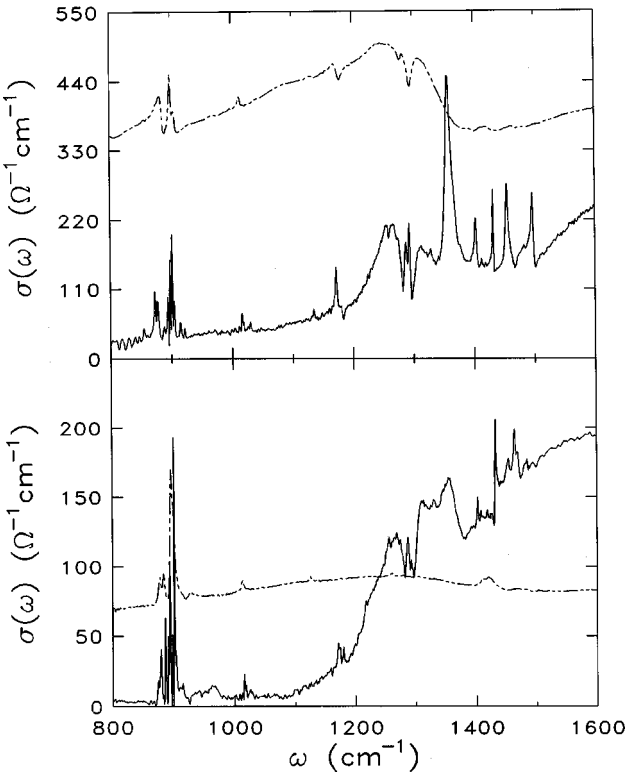

FIG. 8. Upper panel: frequency dependent conductivity of the gap regime in α-$(ET)_3(ReO_4)_2$ in the $\parallel$ polarization at 300 K (dashed line) and 10 K (solid line). Lower panel: frequency dependent conductivity of the gap regime in α-$(ET)_3(ReO_4)_2$ in the $\perp$ polarization at 300 K (dashed line) and 10 K (solid line).

the onset appears at ≈ 1150 cm^{-1} in both polarizations. Previously, this feature was attributed to an interband transition,[11] but more recent work suggests that this low-energy electronic band may be due to an effective Hubbard transition.[40–44]

We also see significant sharpening and splitting of the vibrational features at low temperature, mostly in an approximate $1\rightarrow 2$ ratio. This splitting is especially apparent in Fig. 8, which highlights the gap regime. Unlike the 2:1-phase material, the anion mode at 900 cm^{-1} is significantly hardened and split at 10 K, also in a $1\rightarrow 2$ ratio. Finally, a few weak low-energy lattice modes are observed for α-$(ET)_3(ReO_4)_2$ below 100 cm^{-1}. These features will be discussed in detail in a later section.

C. β-$(ET)_3(ReO_4)_2$

1. Room-temperature spectra

Figure 9 displays the room-temperature reflectance of β-$(ET)_3(ReO_4)_2$ over the entire spectral range. The strong polarization dependence of the spectrum is indicative of a highly anisotropic, quasi-one-dimensional sample. Due to the richness of the spectra taken along the stacking direction (compared to the low, flat, virtually featureless data in the perpendicular direction), we will concentrate our attention on this polarization.

Because of the semiconducting nature of the β complex, the vibrational modes of A_g symmetry are easily identified (see Table I). In addition, the reflectance spectrum of the

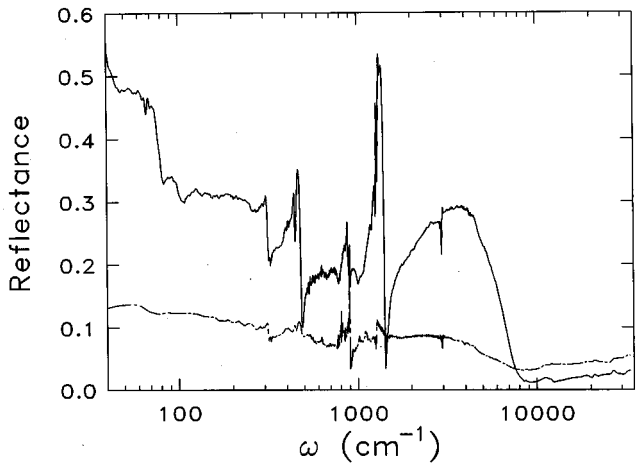

FIG. 9. Room-temperature reflectance spectra of β-$(ET)_3(ReO_4)_2$. Solid line: $\parallel$ polarization; dashed line: $\perp$ polarization.

parallel direction provides clear evidence of a low-lying electronic structure for β-$(ET)_3(ReO_4)_2$, centered near 3000 cm^{-1}. Like the previous two analogs, the main structure near 900 cm^{-1} in the perpendicular direction is attributed to the perrhenate antisymmetric stretch.

The frequency dependent conductivity of β-$(ET)_3(ReO_4)_2$ is shown in Fig. 10. Overall, the spectrum

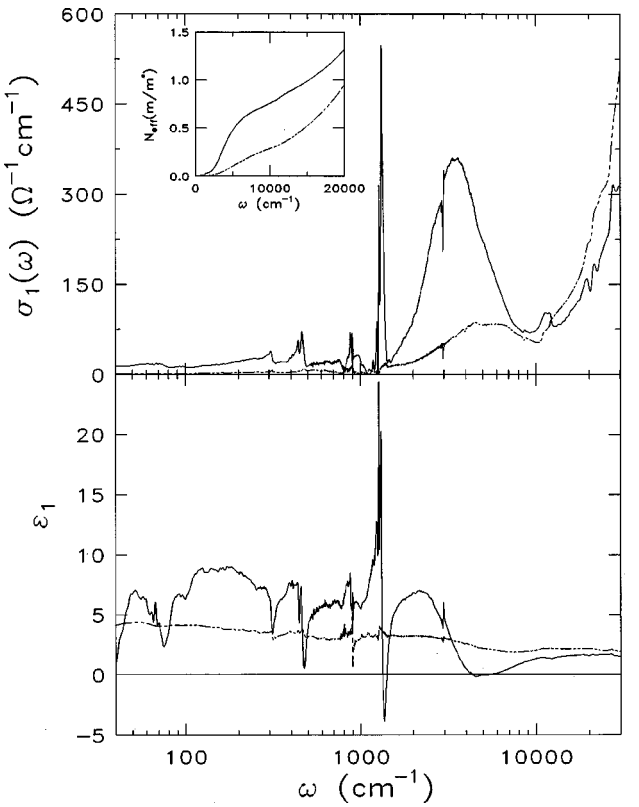

FIG. 10. Top panel: room-temperature conductivity spectra of β-$(ET)_3(ReO_4)_2$. Solid line: $\parallel$ polarization; dashed line: $\perp$ polarization. Inset: 300 K conductivity sum rule as a function of polarization. Bottom panel: room-temperature dielectric constant of β-$(ET)_3(ReO_4)_2$. Solid line: $\parallel$ polarization; dashed line: $\perp$ polarization.

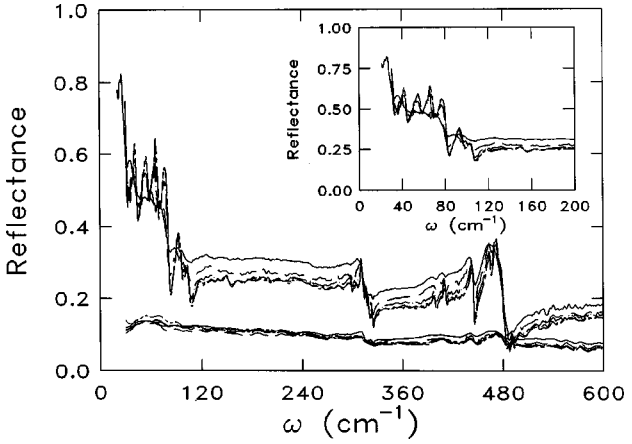

FIG. 11. FIR reflectance spectra of β-$(ET)_3(ReO_4)_2$ as a function of polarization at 10, 70, 140, 230, and 300 K. Inset: close-up view of low-energy modes in the $\|$ direction.

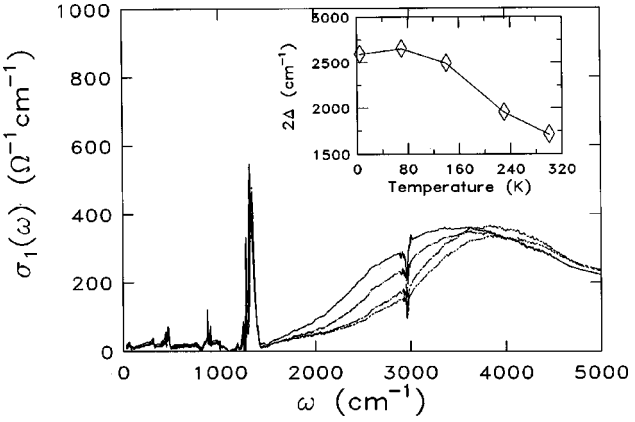

FIG. 12. Frequency dependent conductivity of β-$(ET)_3(ReO_4)_2$ as a function of temperature in the chain axis polarization. Inset: the optical gap 2Δ as a function of temperature.

is characteristic of a semiconductor, with strong vibronic features and a semiconducting gap near 1600 cm^{-1}. The conductivity sum-rule data are shown in the inset of Fig. 10. We estimate $m^* \approx 2.7 m_e$.

The real part of the dielectric function for β-$(ET)_3(ReO_4)_2$ is presented in the lower panel of Fig. 10. In the parallel polarization, we estimate $\epsilon_1(0) \approx 7$, $\omega_p \approx 4300$ cm^{-1}, and $\epsilon_1(\infty) \approx 2.2$. For the perpendicular polarization, $\epsilon_1(0)$ is equal to 4, as expected for a low dielectric semiconductor.

2. Temperature dependence

At low temperatures, β-$(ET)_3(ReO_4)_2$ exhibits modest splitting of the vibronic modes, as well as small changes in overall reflectance levels. In particular, both the central $C=C$ band and the 900-cm^{-1} anion mode show some symmetry breaking, which will be compared with the response of the other perrhenate moieties in Sec. IV. Furthermore, both the low-energy lattice modes and the charge-transfer structure centered near 3000 cm^{-1} display a very systematic temperature dependence, as described below.

In the β crystal, we observe a series of fairly sharp features in the low-temperature FIR spectrum (Fig. 11). We assign these structures as lattice modes of β-$(ET)_3(ReO_4)_2$. Note that the strong polarization dependence of these modes is a direct result of the quasi-one-dimensional structure of the sample. Although weakly present at room temperature, the lattice modes gradually increase in intensity on passing through the structural phase transition. This behavior is indicative of a weak, second-order, semiconductor $\rightarrow$ semiconductor transition between 140 and 230 K, likely near 150 K.

As expected for a quasi-one-dimensional, semiconducting material, the charge-transfer band is readily apparent at low temperatures in the conductivity plot (Fig. 12). At 10 K, we estimate $2\Delta \approx 2600$ cm^{-1}. As can be seen from the inset, the size of the gap changes systematically with temperature, again pointing to a second-order semiconductor $\rightarrow$ semiconductor structural phase transition between 140 and 230 K for β-$(ET)_3(ReO_4)_2$.

IV. DISCUSSION

The perrhenate family of salts provides an important opportunity to examine chemical and structural effects on the physical properties in ET-based organic molecular solids. Here, we concentrate on a comparison of phase-transition mechanisms as well as the factors which work to stabilize the superconducting ground state in the 2:1 analog. Our spectroscopic data are also compared with previous results on $(TMTSF)_2ReO_4$.

A. Vibrational features

It is well known that a distortion of the unit cell will reduce the local symmetry and remove phonon degeneracies, with the nature of the multiplet splitting in the infrared providing information on how the degeneracy is removed. In organic solids, the A_g coupling-induced vibrational modes provide especially sensitive (and highly directional) indicators of changing crystal structure and chemical interactions through a phase transition, with vibrational splittings signaling the symmetry environment of the low-temperature phase.

The clearest example of vibronic symmetry breaking in the perrhenate family is shown in Figs. 7 and 8, where the vibrational modes in α-$(ET)_3(ReO_4)_2$ become significantly hardened and split in the low-temperature phase, usually in a $1 \rightarrow 2$ ratio. We attribute this result to massive symmetry breaking of the ET molecules through the phase transition, likely driving them far from planar symmetry. These contortions may, in fact, keep α-$(ET)_3(ReO_4)_2$ from achieving the superconducting ground state found in the 2:1 phase. Such a multiplet splitting pattern indicates a doubling of the unit cell in the α material. It is notable that there is significantly less symmetry breaking of vibronic modes in both the β-3:2 and the 2:1 materials. For $(ET)_2ReO_4$, the weak splitting behavior occurs primarily in the FIR. The lack of strong multiplet splitting in the 2:1 compound argues against a change in the unit-cell size at 82 K, in contrast with previous structural results.[10]

The structure in the central $C=C$ region near 1200 cm^{-1}, which often dominates the infrared spectrum of ET-based organic solids in the parallel direction, shows some amount of symmetry breaking in all samples (Fig. 13). As expected,

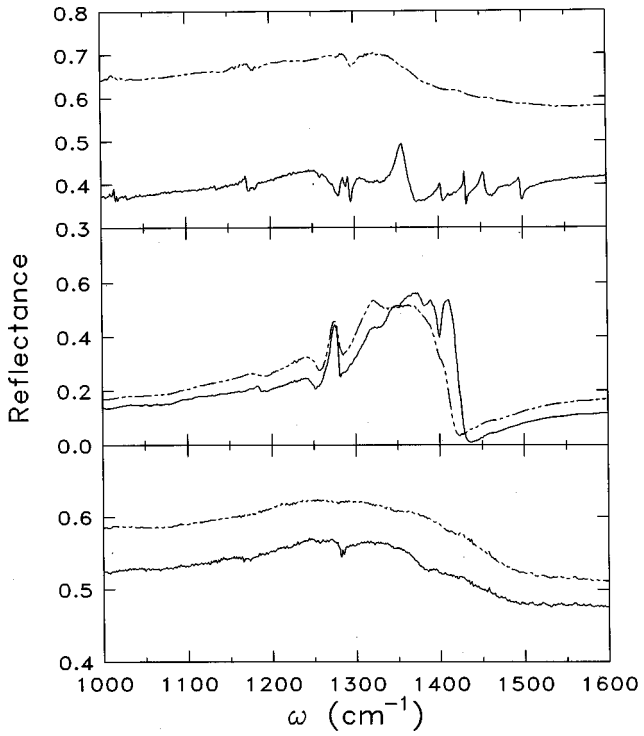

FIG. 13. Reflectance in the $C=C$ regime at 300 K (dashed line) and 10 K (solid line) in the high-conductivity direction for α-$(ET)_3(ReO_4)_2$ (top panel), β-$(ET)_3(ReO_4)_2$ (middle panel), and $(ET)_2(ReO_4)$ (bottom panel).

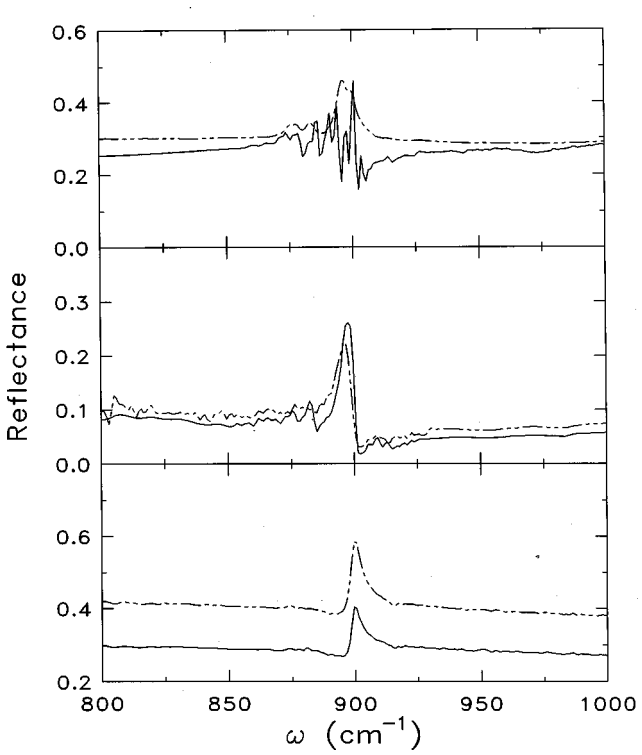

FIG. 14. 300 K (dashed line) and 10 K (solid line) reflectance spectra of the anion mode for α-$(ET)_3(ReO_4)_2$ (top panel), β-$(ET)_3(ReO_4)_2$ (middle panel), and $(ET)_2(ReO_4)$ (bottom panel).

this splitting and sharpening is most apparent in the α crystal. It is moderate in the β-phase material, with a weak splitting of this area on the high-energy side, near 1400 cm^{-1}. However, the symmetry breaking in the $C=C$ region for the 2:1 sample is significantly less than for the two aforementioned 3:2 compounds, with the only change at 10 K being the development of a dip in the reflectance near 1280 cm^{-1}.

In order to assess the role of counterion ordering on the phase-transition mechanisms in the α, β, and 2:1 materials, we compare the infrared response near 900 cm^{-1} (Fig. 14), where the antisymmetric stretch of the anion mode is observed. This perrhenate mode displays significant low-temperature splitting in both the α and β salts, hardening and splitting in a $1\rightarrow 2$ ratio at low temperature in the α-phase compound and exhibiting a weak multiplet splitting in the β-phase solid. This suggests that the respective phase transitions in α-$(ET)_3(ReO_4)_2$ and β-$(ET)_3(ReO_4)_2$ are driven by anion ordering, in agreement with previous ESR work.[9]

In contrast, the ReO_4 antisymmetric stretch near 900 cm^{-1} undergoes little change at T_c in the 2:1 analog (Fig. 14). Thus we conclude that the role of anion reordering in $(ET)_2(ReO_4)$ is minimal compared with the aforementioned 3:2 samples. This result is in contrast to previous ESR work and in line with the more recent structural analysis of Ravy *et al.*[9,10] While it is unlikely that the metal $\rightarrow$ insulator transition in the 2:1 material is anion driven because of the complete lack of change of the 900-cm^{-1} mode through the phase transition, a very modest role for the anion cannot be completely ruled out. This is because a quartet of peaks, associated with ReO_4 contortions in $(TMTSF)_2(ReO_4)$, also appears in our $(ET)_2(ReO_4)$ low-temperature spectra.[36] It is, however, impossible to tell whether they are split or not (compared to the high-temperature phase response) because they are not observed above the phase transition.

The splitting behavior of the 900-cm^{-1} anion mode of the materials in this study is summarized in Table II along with results of a few related compounds. To recap, the 82-K metal

TABLE II. Summary of 900-cm^{-1} anion mode activity at low-temperature for several perrhenate containing complexes.

Molecule	Low-temperature behavior of anion mode
α-$(ET)_3(ReO_4)_2$	Split into doublets
β-$(ET)_3(ReO_4)_2$	Moderately strong splitting into five peaks
$(ET)_2(ReO_4)$	No splitting, very little hardening
$(TMTSF)_2(ReO_4)$	Peaks split into at least doublets, possibly triplets (Ref. 36)
$(BEDO\text{-}TTF)_2(ReO_4)(H_2O)$	Detailed behavior not reported in (Ref. 47)

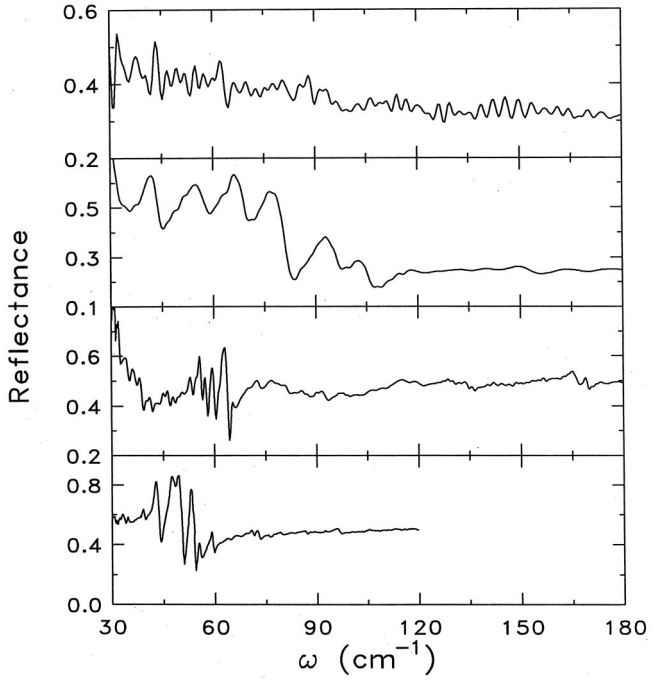

FIG. 15. 10-K reflectance spectra in the high-conductivity direction of very FIR lattice modes in α-$(ET)_3(ReO_4)_2$ (top panel), β-$(ET)_3(ReO_4)_2$ (second panel). $(ET)_2(ReO_4)$ (third panel), and $(TMTSF)_2(ReO_4)$ (bottom panel). Note that the $(TMTSF)_2(ReO_4)$ data was reproduced with permission of the authors from Ref. 38.)

$\rightarrow$ insulator transition in the 2:1 sample involves a weak structural modification rather than counterion ordering as in the α- and β-3:2 samples. The fact that the spectra of $(ET)_2(ReO_4)$ display no strong symmetry breaking, especially in the middle infrared, suggests that this is a very weak displacive phase transition[10] quite different from that of $(TMTSF)_2(ReO_4)$ where anion ordering effects are dominant.[36] The correlation between these changes and the occurrence of superconductivity is not yet known, but clearly the low-temperature phase of $(ET)_2(ReO_4)$ is the ''parent phase'' of the superconductivity, whereas the superconducting ground state is not observed in the TMTSF-based material. Recently, the metal $\rightarrow$ semiconductor phase transition in $(BEDO\text{-}TTF)_2ReO_4(H_2O)$ has also been attributed to anion ordering. Unlike the 2:1 ET perrhenate, however, 300-K structural data indicate a slight disorder of the counterions.[45–48]

B. Lattice modes

Figure 15 displays a comparison of the FIR spectra of the three ET moieties of interest in this study, along with that of $(TMTSF)_2(ReO_4)$.[38] Like the aforementioned vibronic features, the amplitude and number of low-energy lattice modes are a major aspect of the richness and diversity of the perrhenate series. Thus we briefly compare the systems.

The upper two panels of Fig. 15 display the FIR response along the high-conductivity direction of the α and β 3:2 samples. The lattice modes in β-$(ET)_3(ReO_4)_2$ are both larger in amplitude and greater in number than those of α-$(ET)_3(ReO_4)_2$, highlighting one primary distinction between the two 3:2 moieties. Combined with dimensionality considerations, the different lattice mode response may partially explain the semiconducting response of the β-phase compound as these motions of the lattice can provide a low-energy distortion mechanism. In β-$(ET)_3(ReO_4)_2$, the lattice modes are also sensitive to the structural phase transition, as mentioned previously.

TABLE III. 300-K effective mass (m^*), 300-K screened plasma frequency (ω_p), 10-K optical gap (2Δ), and U_{eff} estimated at 10 K for $(ET)_2(ReO_4)$, α-$(ET)_3(ReO_4)_2$, and β-$(ET)_3(ReO_4)_2$.

Material	m^* [a]	ω_p (cm^{-1})	2Δ (cm^{-1})	U_{eff} (cm^{-1})
$(ET)_2(ReO_4)$	$2.9m_e$	4720	480	1250
α-$(ET)_3(ReO_4)_2$	$2.2m_e$	4250	1150	2200
β-$(ET)_3(ReO_4)_2$	$2.7m_e$	4300	2600	3710

The lower two panels of Fig. 15 show the FIR response of the 2:1 sample together with that of the analogous 2:1 TMTSF material.[38] The sharp lattice modes observed in $(ET)_2(ReO_4)$ are very similar in character to those of $(TMTSF)_2(ReO_4)$, although the TMTSF features are of larger amplitude and lower energy. The amplitude of the low-energy lattice vibrations in the TMTSF salt may prevent the system from achieving a superconducting ground state (like the ET counterpart) because these modes provide a mechanism for low-energy distortions of a soft lattice. In addition, the reflectance in the ET-based material rises significantly below 45 cm^{-1}, in line with the ''nearly superconducting'' behavior of $(ET)_2ReO_4$.

C. Electronic structure

In all three perrhenate compounds, a broad electronic feature dominates the 300-K infrared spectra. The two-dimensional aspects of the band structure have motivated the assignment of such low-lying electronic bands as interband transitions in a number of organic solids. Indeed, this feature was attributed to an interband transition in α-$(ET)_3(ReO_4)_2$, due to the lack of dispersion from charge transfer in the near-infrared region of the spectrum in an earlier investigation.[11] The interband interpretation is frequently cited in organic solids, but another attractive scenario is that the electronic gap feature is due to an effective Hubbard gap or an Abrikosov-Suhl resonance.[40–44,49,50] Such structures are known to arise in strongly correlated systems near the Mott transition, where a one-electron band picture breaks down. Although strictly intended for the κ-phase ET systems with strong dimeric units, the effective Hubbard gap model is likely valid in spirit for other packing geometries, although it may be lacking in the particulars for such situations. For instance, the FIR structure in $(TMTSF)_2(PF_6)$ has recently been assigned based on a Hubbard gap view.[51]

In our materials, the effective Hubbard gap assignment is supported by estimates of the effective mass (m^*) obtained from the conductivity sum rule (Table III). Here, the values of m^* suggest that electron correlation is relatively important in the 2:1, α, and β solids. Photoemission measurements on similar materials also support the supposition of a highly correlated state.[52] At the same time, the overall character of the spectra show that localization effects are also significant. The breadth and temperature dependence of this feature also argue in favor of the Hubbard assignment. Interpretation of

the low-lying electronic feature as an excitation over an effective Hubbard gap is therefore reasonable for 2:1, α, and β perrhenate compounds studied here, and within this model one can extract an experimental measure of the effective on-site Coulomb interaction, U_{eff} (Table III). Certainly, explanations based on charge-transfer, Hubbard gap, or interband transitions illustrate the range of possible interpretations of the electronic structure in organic solids, with strong electronic correlations playing a major role in the assignment of a Hubbard gap (or Abrikosov-Suhl resonance) and low correlations important in a band-structure view. This subject is open to further experimentation and debate, particularly with regard to the Coulombic or phononic nature of correlations in ET salts.

Although the low-temperature ground state for each material is semiconducting (Table III), there are still important differences in the overall electronic behavior. For the 2:1 and α salts, weak metallic behavior is observed in the high-temperature phases and the gap opens up only below T_c in each compound. Gap formation is rapid, and 2Δ occurs in the middle infrared. In the β salt, the optical gap is fairly large as expected for quasi-one-dimensional semiconductor, with 2Δ changing gradually through the semiconducting $\rightarrow$ semiconducting structural phase transition.

V. CONCLUSION

We have investigated the polarized infrared and optical reflectance of several members of the ET/perrhenate family of organic molecular solids as a function of temperature. The low-temperature phase of each material is characterized by the opening of a semiconducting gap and symmetry breaking, as evidenced by vibrational fine structure in varying degrees. Anion ordering drives the phase transition in the α- and β-3:2 materials, whereas $(ET)_2(ReO_4)$ has a weak structural modification at T_c which is most likely not anion related, with mode splittings occurring primarily in the FIR. Correlation effects play an important role in the low-lying electronic structure for the three moieties, and we suggest that a Hubbard gap picture may be appropriate.

ACKNOWLEDGMENTS

Financial support from the Division of Materials Research (Grant No. DMR-9623221) of the National Science Foundation is gratefully acknowledged. Research at Argonne National Laboratory was supported by the U.S. Department of Energy, Office of Basic Energy Sciences, Division of Materials Sciences, under Contract No. W-31-109-ENG-38. S.M.B. thanks the Dean's Office at SUNY-Binghamton for funding. The authors also thank Katalin Kamarás for use of an IR microscope to check the absolute reflectance level of our 2:1 crystal and David Dwyer for assistance in determining 300-K ESR linewidths. This work benefited from many useful conversations with Chris Homes, Katalin Kamarás, and Akito Ugawa. The spectra of $(TMTSF)_2(ReO_4)$ in Fig. 15 is reproduced here with permission of Chris Homes. We thank Virginia Long for her careful reading of the manuscript.

[1] K.D. Carlson, U. Geiser, A.M. Kini, H.H. Wang, L.K. Montgomery, W.K. Kwok, M.A. Beno, J.M. Williams, C.S. Cariss, G.W. Crabtree, M.-H. Whangbo, and M. Evain, Inorg. Chem. **27**, 965 (1988).

[2] J.M. Williams, J.R. Ferraro, K.D. Carlson, U. Geiser, H.H. Wang, A.M. Kini, and M.-H. Whangbo, *Organic Superconductors (Including Fullerenes): Synthesis, Structure, Properties, and Theory* (Prentice Hall, Englewood Cliffs, NJ, 1992).

[3] A.M. Kini, U. Geiser, H.H. Wang, K.D. Carlson, J.M. Williams, W.K. Kwok, K.G. Vandervoort, J.E. Thompson, D.L. Stupka, D. Jung, and M.-H. Whangbo, Inorg. Chem. **29**, 2555 (1990).

[4] U. Geiser, J.A. Schlueter, H.H. Wang, A.M. Kini, J.M. Williams, P.P. Sche, J.I. Zakowicz, M.L. VanZile, J.D. Dudek, P.G. Nixon, R.W. Winter, G.L. Gard, J. Ren, and M.-H. Whangbo, J. Am. Chem. Soc. **118**, 9996 (1996).

[5] J.A. Schlueter, K.D. Carlson, U. Geiser, H.H. Wang, J.M. Williams, W.-K. Kwok, J.A. Fendrich, U. Welp, P.M. Keane, J.D. Dudek, A.S. Komosa, D. Naumann, T. Roy, J.E. Schirber, W.R. Bayless, and B. Dodrill, Physica B **233**, 279 (1994).

[6] T. Burgin, T. Miebach, J.C. Huffman, L.K. Montgomery, J.A. Paradis, C. Rovira, M-H. Whangbo, S.N. Magonov, S.I. Khan, C.E. Strouse, D.L. Overmyer, and J.E. Schirber, J. Mater. Chem. **5**, 1659 (1995).

[7] S.S.P. Parkin, E.M. Engler, R.R. Schumaker, R. Lagier, V.Y. Lee, J. Voiron, K. Carneiro, J.C. Scott, and R.L. Greene, J. Phys. (Paris), Colloq. **44**, C3-791 (1982).

[8] S.S.P. Parkin, E.M. Engler, R.R. Schumaker, R. Lagier, V.Y. Lee, J.C. Scott, and R.L. Greene, Phys. Rev. Lett. **50**, 270 (1983).

[9] K. Carneiro, J.C. Scott, and E.M. Engler, Solid State Commun. **50**, 477 (1984).

[10] S. Ravy, R. Moret, J.P. Pouget, R. Comes, and S.S.P. Parkin, Phys. Rev. B **33**, 2049 (1986).

[11] K. Yakushi, H. Kanbara, H. Tajima, H. Kuroda, G. Saito, and T. Mori, Bull. Chem. Soc. Jpn. **60**, 4251 (1987).

[12] E.M. Engler, V.Y. Lee, R.R. Schumaker, S.S.P. Parkin, R.L. Greene, and J.C. Scott, Mol. Cryst. Liq. Cryst. **107**, 19 (1984).

[13] K. Yamaji, Solid State Commun. **61**, 413 (1987).

[14] H. Kobayashi, R. Kato, T. Mori, A. Kobayashi, Y. Sasaki, G. Saito, T. Enoki, and H. Inokuchi, Mol. Cryst. Liq. Cryst. **107**, 33 (1984).

[15] J.M. Williams, M.A. Beno, H.H. Wang, P.E. Reed, L.A. Azevedo, and J.E. Schirber, Inorg. Chem. **23**, 1790 (1984).

[16] T. Ishiguro and K. Yamaji, *Organic Superconductors* (Springer-Verlag, New York, 1989), Chap. 5.

[17] P.C.W. Leung, M.A. Beno, U. Geiser, H.H. Wang, and J.M. Williams, Mol. Cryst. Liq. Cryst. **141**, 117 (1986).

[18] H. Kanbara, H. Tajima, S. Aratani, K. Yakushi, H. Kuroda, G. Saito, A. Kawamoto, and J. Tanaka, Chem. Lett. **1986**, 437.

[19] C.S. Jacobsen, J.M. Williams, and H.H. Wang, Solid State Commun. **54**, 937 (1985).

[20] H. Kuroda, K. Yakushi, H. Tajima, and G. Saito, Mol. Cryst. Liq. Cryst. **125**, 135 (1985).

[21] J. Dong, J.L. Musfeldt, J.A. Schlueter, J.M. Williams, and G.L. Gard (unpublished).

[22] C.S. Jacobsen, D.B. Tanner, J.M. Williams, U. Geiser, and H.H. Wang, Phys. Rev. B **35**, 9605 (1987).
[23] It should be noted that the α phase typically forms crystals that are thinner and more brittle than the others in this study.
[24] F. Wooten, *Optical Properties of Solids* (Academic Press, New York, 1972).
[25] A unit cell having dimensions of $a=8.498$ Å, $b=30.566$ Å, and $c=9.413$ Å ($V=2443.87$, $Z=2$ was used for both the α and β calculations. Note that these data are exact for the α phase and only approximate for the β phase. The 2:1 phase has unit-cell dimensions of $a=7.78$ Å, $b=12.59$ Å, and $c=16.79$ ($V=1565$ Å^3, $Z=2$).
[26] M.J. Rice, V.M. Yartsev, and C.S. Jacobsen, Phys. Rev. B **21**, 3437 (1980).
[27] M.J. Rice, Phys. Rev. Lett. **37**, 36 (1976).
[28] M.J. Rice, Solid State Commun. **31**, 91 (1979).
[29] J. Hubbard, Phys. Rev. B **17**, 494 (1978).
[30] M.E. Kozlov, K.I. Pokhodnia, and A.A. Yurchenko, Spectrochim. Acta A **43**, 323 (1987).
[31] M.E. Kozlov, K.I. Pokhodnia, and A.A. Yurchenko, Spectrochim. Acta A **45**, 437 (1989).
[32] J.E. Eldridge, C.C. Homes, J.M. Williams, A.N. Kini, and H.H. Wang, Spectrochim. Acta A **51**, 947 (1995).
[33] M. Meneghetti, R. Bozio, and C. Pecile, J. Phys. (France) **47**, 1377 (1986).
[34] J.E. Eldridge, Y. Xie, H.H. Wang, J.M. Williams, A.M. Kini, and J.A. Schlueter, Spectrochim. Acta A **52**, 45 (1996).
[35] J.E. Eldridge, Y. Xie, Y. Lin, C.C. Homes, H.H. Wang, J.M. Williams, A.M. Kini, and J.A. Schlueter, Spectrochim. Acta A **53**, 565 (1997).
[36] C.C. Homes and J.E. Eldridge, Phys. Rev. B **42**, 9522 (1990).
[37] J.L. Musfeldt, C.C. Homes, M. Almeida, and D.B. Tanner, Phys. Rev. B **46**, 8777 (1992).
[38] C.C. Homes and J.E. Eldridge, Phys. Rev. B **40**, 6138 (1989).
[39] H. Kuroda, K. Yakushi, H. Tajima, H. Kanbara, and G. Saito, Mol. Cryst. Liq. Cryst. **19**, 131 (1987).
[40] A. Kawamoto, K. Miyagawa, Y. Nakazawa, and K. Kanoda, Phys. Rev. B **52**, 15 522 (1995).
[41] K. Kanoda, Physica C **282**, 299 (1997).
[42] A. Fortunelli and A. Painelli, Synth. Met. **85**, 1631 (1997).
[43] R.H. McKenzie, J. Phys.: Condens. Matter (to be published).
[44] R.H. McKenzie, Science **278**, 820 (1997).
[45] S. Kahlich, D. Schweitzer, I. Heinen, Song En Lan, B. Nuber, H.J. Keller, K. Winzer, and H.W. Helberg, Solid State Commun. **80**, 191 (1991).
[46] S. Kahlich, D. Schweitzer, P. Auban-Senzier, D. Jérome, and H.J. Keller, Solid State Commun. **83**, 77 (1992).
[47] E. Grießhaber, J. Moldenhauer, D. Schweitzer, I. Heinen, H.J. Keller, and W. Strunz, Synth. Met. **87**, 11 (1997).
[48] S.S. Khasanov, B.Zh. Narymbetov, L.V. Zorina, L.P. Rozenberg, R.P. Shibaeva, N.D. Kushch, E.B. Yagubskii, R. Rousseau, and E. Canadell, Eur. Phys. J. B **1**, 419 (1998).
[49] B.R. Bulka, Mol. Phys. Rep. (to be published).
[50] Th. Pruschke, D.L. Cox, and M. Jarrell, Phys. Rev. B **47**, 3553 (1993).
[51] J. Favand and F. Mila, Phys. Rev. B **54**, 10 425 (1996).
[52] A. Sekiyama, T. Susali, A. Fujimori, T. Sasaki, N. Toyota, T. Kondo, G. Saito, M. Tsunekawa, T. Iwasaki, T. Mura, T. Mutsishita, S. Suga, H. Ishii, and T. Miyahara, Phys. Rev. B **56**, 9082 (1997).